Classical Aspects in Above-Threshold Ionization with a Midinfrared Strong Laser Field

W. Quan,[1] Z. Lin,[1] M. Wu,[1] H. Kang,[1] H. Liu,[1] X. Liu,[1,*] J. Chen,[2,3,†] J. Liu,[2,3] X. T. He,[2,3] S. G. Chen,[3] H. Xiong,[4] L. Guo,[4] H. Xu,[4] Y. Fu,[4] Y. Cheng,[4,‡] and Z. Z. Xu[4,§]

[1]*State Key Laboratory of Magnetic Resonance and Atomic and Molecular Physics, Wuhan Institute of Physics and Mathematics, Chinese Academy of Sciences, Wuhan 430071, China*

[2]*Center for Applied Physics and Technology, Peking University, Beijing 100084, China*

[3]*Institute of Applied Physics and Computational Mathematics, P.O. Box 8009, Beijing 100088, China*

[4]*State Key Laboratory of High Field Laser Physics, Shanghai Institute of Optics and Fine Mechanics, Chinese Academy of Sciences, P.O. Box 800-211, Shanghai 201800, China*

(Received 5 January 2009; revised manuscript received 26 March 2009; published 24 August 2009; publisher error corrected 31 August 2009)

We present high resolution photoelectron energy spectra of noble gas atoms from high intensity above-threshold ionization (ATI) at midinfrared wavelengths. An unexpected structure at the very low-energy portion of the spectra, in striking contrast to the prediction of the simple-man theory, has been revealed. A semiclassical model calculation is able to reproduce the experimental feature and suggests the prominent role of the Coulomb interaction of the outgoing electron with the parent ion in producing the peculiar structure in long wavelength ATI spectra.

DOI: 10.1103/PhysRevLett.103.093001 PACS numbers: 32.80.Rm, 32.80.Wr, 42.50.Hz

When exposed to a strong laser field, atoms may absorb more photons than necessary for ionization, leading to a series of peaks separated by one photon energy in the photoelectron spectrum. This process, coined as above-threshold ionization (ATI), was discovered almost 30 years ago [1]. Since then, ATI has been continuously advancing our understanding of strong-field physics [2].

One of the most prominent features in ATI, in the long wavelength, high intensity limit, is the rapid decay of the ionization rate with the electron energy in the low-energy part of the photoelectron spectrum, followed by a high-energy plateau [3] extending up to $10U_p$ ($U_p = I/4\omega^2$, denotes the ponderomotive energy, where I is the laser intensity and ω the frequency). The physical insight therein was found to be rooted in a rather simple semiclassical simple-man description of the ionization process [4], based on the pioneering work by Keldysh [5]. Here, a pivotal role is given to the Keldysh parameter $\gamma = \sqrt{I_p/2U_p}$, where I_p is the ionization potential. Under the condition of $\gamma \ll 1$, the simple-man picture of the ionization dynamics may be verified. Therein, the motion of the active electron, initially tunnel ionized, is entirely determined by its interaction with the laser electric field, while the effect of the binding potential is neglected.

Despite the great success and pivotal role of this intuitive semiclassical picture in understanding ATI processes of atoms in the strong field, many puzzles still exist. For example, the photoelectron spectra of argon show a resonancelike structure at intermediate electron energy [6], which is beyond the scope of the semiclassical picture and still under debate [7]. Furthermore, recent experiments using the sophisticated cold target recoil-ion momentum spectroscopy (COLTRIMS) show a clear minimum at zero in the electron momentum distribution along the laser polarization direction [8], obviously deviating from the prediction of the simple-man theory [4]. Theoretical studies with the semiclassical approach [9,10] have been focused on this peculiar low electron momentum structure, suggesting a prominent role of the Coulomb potential. However, further COLTRIMS experiments [11,12] reveal many resonancelike peaks in the electron momentum distribution, a characteristic of the multiphoton ionization (MPI). As these experiments were mostly performed at 800 nm wavelength, one difficulty one may encounter is to reliably stay in the regime in which the semiclassical picture is valid (i.e., $\gamma \ll 1$).

In principle, the semiclassical regime could be easily reached by increasing the laser wavelength, compared to the intensity, considering the fact that $U_p \propto I\lambda^2$. Thanks to the advances in ultrafast laser technology, tunable long wavelength lasers with focusable peak intensities around 10^{14} W/cm^2 have become available recently, providing a potential for going deeply into the tunnel regime without saturated ionization of target atoms or molecules. Indeed, a pioneering experiment with midinfrared wavelengths has been performed very recently and a λ^2 scaling of the classical behavior both in ATI and closely related high harmonic generation was observed [13], enabling the classical limit to be approached with unprecedented power.

In this Letter, we present the ATI spectra of noble gas atoms in ultrashort intense laser pulses at midinfrared wavelengths. In particular, the application of long wavelength provides the opportunity to go deep in the semiclassical regime, exploring the classical aspects in strong-field physics more closely. Indeed, our data at long wavelengths show a pronounced structure in the very low-energy part of photoelectron spectra. While this finding is in striking

 © 2009 The American Physical Society

contrast to the prediction of the simple-man theory, a simulation based on a semiclassical model is able to reproduce this feature qualitatively and suggests it as a classical aspect in ATI at long wavelengths.

In our experiments, wavelength-tunable midinfrared femtosecond laser pulses are generated by an optical parametric amplifier (OPA, TOPAS-C, Light Conversion, Inc.) pumped by a commercial Ti:sapphire laser system (Legend, Coherent, Inc.) [14]. The pulse energy from OPA is variable, before focused into the vacuum chamber, by means of an achromatic half wave plate followed by a polarizer. The photoelectron energy spectra are measured with a field-free time-of-flight spectrometer. By means of a cryopump, the base pressure of the spectrometer is maintained below 10^{-8} mbar. Photoionized electrons are detected by microchannel plates that subtend a 5° angle at the light-atom interaction point, and are recorded by a multihit time-to-digital converter with an ultimate resolution of 25 ps (TDC8HP, Roentdek Handels GmbH). An energy resolution of about 20 meV for 1 eV electrons has been measured for this spectrometer.

Figures 1(a), 1(c), and 1(e) show the low-energy part of the measured photoelectron spectra of xenon at different laser wavelengths and intensities. The data at longer wavelengths, e.g., 1500 and 2000 nm, reveal a pronounced structure at very low electron energy. This structure seemingly consists of two humps at higher laser intensities [see Figs. 1(c) and 1(e)]. The first hump lies at electron energy below 1 eV, while the second broader one at slightly higher electron energy exhibits a strong dependence on both the laser wavelength and intensity. At the shortest wavelength of 800 nm, the latter is hardly seen, while distinct resonant structures within each ATI order, an indication that the MPI process is dominant, become prominent. We note that this feature is also present for the other noble gas species we have studied, e.g., krypton and argon, and thus seems to be a universal phenomenon for high intensity ATI spectra at long wavelengths.

This peculiar low-energy structure, which becomes more significant at 2000 nm, is in striking contrast to the prediction of the simple-man theory, while, with which, the overall evolution of the ATI spectra, e.g., the appearance of the well-known plateau [3] and an approximately quadratically increase of the 10 U_p cutoff with the laser wavelength λ, is well predicted [see the inset in Fig. 1(a)]. In the remaining part of this Letter, we will focus on this feature at long wavelengths, with emphasis on the second hump.

One major question concerns whether the second hump that well develops at long wavelengths, e.g., 2000 nm, is a classical aspect in the ATI spectra, as for the well-established high-energy plateau. We address this question by comparing the experimental data with the results of the theoretical simulations based on a semiclassical description of the ionization process.

Details of the semiclassical approach have been described elsewhere [15]. In brief, we consider a xenon

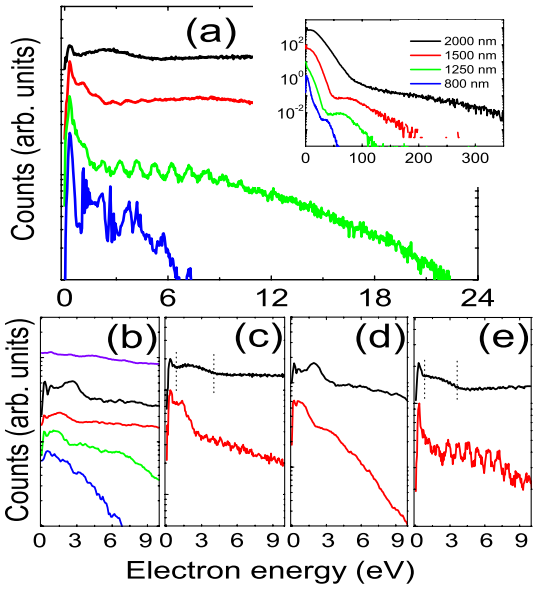

FIG. 1 (color online). Experimental [(a), (c), and (e)] and calculated [(b),(d)] photoelectron spectra of xenon. (a) $I = 8.0 \times 10^{13}$ W/cm^2, $\lambda = 800$, 1250, 1500, and 2000 nm from bottom to top, respectively. The complete spectra are shown in the inset. The laser pulse durations are ~40 fs at 800 nm, ~30 fs at 1250 and 1500 nm, while ~90 fs at 2000 nm. (b) $I = 8.0 \times 10^{13}$ W/cm^2 and $\lambda = 800$, 1250, 1500, and 2000 nm, with Coulomb potential for the curves from bottom to top, respectively. While the uppermost curve is for $I = 8.0 \times 10^{13}$ W/cm^2 and $\lambda = 2000$ nm without Coulomb potential. (c),(d) $\lambda = 2000$ nm, $I = 3.2$, 6.4×10^{13} W/cm^2 for the lower and upper curves, respectively. (e) $\lambda = 1500$ nm, $I = 4.0$, 10.0×10^{13} W/cm^2 for the lower and upper curves, respectively. In (c) and (e), the boundaries of the second hump are indicated by the dashed lines for higher intensities. The curves are shifted in the vertical direction for visual convenience.

atom (with hydrogenlike potential of $V = -Z_{\text{eff}}/r$ where Z_{eff} is the effective nuclear charge) interacting with an external laser field. The laser field $\epsilon(t) = f(t)E_0 \cos\omega t$ has a constant amplitude for the first ten cycles and is ramped off within 3-cycles. For simplification, the electron is released within the time interval $-\pi/2 \leq \omega t \leq \pi/2$ through tunneling with a rate given by the ADK formula [16]. The subsequent evolution of the electron is determined by Newton's equation of motion. This model has achieved great success in explaining various strong-field ionization phenomena [15] under the circumstances that the semiclassical picture can be verified, which should be the case for our long wavelength data (e.g., $\gamma = 0.45$ at 2000 nm and 8×10^{13} W/cm^2).

In Figs. 1(b) and 1(d), the calculated photoelectron spectra of xenon at various wavelengths and intensities are shown. To compare directly with the data, in the calculation, we select out only those electrons emitted along the field direction. In general, the calculation reproduces qualitatively the overall features in the data at long wavelengths, i.e., a pronounced low-energy structure, the

separation into two humps, and the significance of the second hump with the increase of the intensity and wavelength. For shorter wavelengths, the discrepancy between the data and simulation becomes non-negligible. This may not be a surprise, considering the fact that the MPI mechanism, which is beyond the scope of the semiclassical treatment, becomes prominent. Note that the first hump can also be reproduced to some extent at long wavelengths in the simulation. However, the persistence of this hump structure in the data even at, e.g., 800 nm, indicates that other mechanisms may play a role at shorter wavelengths, which is still under investigation. Upon the reasonable agreement at long wavelengths, one may conclude that the peculiar low-energy structure is a pure classical aspect in strong-field single ionization. Moreover, the calculated result without including the Coulomb potential, as shown in Fig. 1(b), shows that the structure completely disappears. In the following, we will further demonstrate that the structure is a consequence of the Coulomb interaction between the electron and the parent ion [17]. Note that the influence of Coulomb potential on single ionization of atoms has been studied at laser wavelength of 800 nm recently [9,10,18].

In order to facilitate the analysis, we present the calculated density plot of the two-dimensional electron momentum distributions, and classify the electron trajectories that contribute to the distributions into two categories, i.e., direct electrons and the indirect ones, by their initial tunneling ionization times. In the context of simple-man theory, the direct electron is tunnel ionized in the rising edge, i.e., $\omega t \in [-\pi/2, 0]$, of the oscillating laser electric field, and leaves directly without further interaction with the ion core. In contrast, the indirect one may return and collide with the core after initially ionized in the falling edge ($\omega t \in [0, \pi/2]$). It is well known that the latter one, if backscattered upon the ion core, produces the high-energy plateau in ATI spectra [3]. Moreover, to reveal the distinct role of the Coulomb potential for direct and indirect electrons, respectively, we compare the results with and without including the Coulomb potential.

Figures 2(a) and 2(c) depict the two-dimensional momentum distributions for electrons initially tunnel ionized in the rising and falling edges of the oscillating laser electric field, respectively, without including the Coulomb potential. Not surprisingly, the results show that most electrons are distributed around momentum of zero, in both parallel and perpendicular directions with respect to the laser polarization, in accordance with the simple-man model.

In Figs. 2(b) and 2(d), the calculations are made with the Coulomb interaction included. It is obvious that the overall momentum distribution in the direction perpendicular to the laser electric field is much narrower than that without considering the Coulomb potential and, in particular, the electrons even concentrate in the field direction in the low momentum region. For both the rising and falling edges, one sees that the momentum distributions clearly shift in the laser polarization direction. This shift can be understood as the overall influence of the Coulomb potential on the wave packet's longitudinal momentum of the electron as it leaves the saddle point after tunneling. Moreover, for the rising edge, the ionized electrons are accumulated in a small region which is close to, but deviates from, zero momentum. The energy position of this highly distributed region is in accordance with the first hump in the photoelectron spectra. For the falling edge, the electrons are accumulated in two small regions. One is close to zero while its center position is in between the two main humps in the calculated photoelectron spectra, which is, however, not distinguishable in the data. The other one is wider in the direction of the field and centers around 0.42 a.u., which corresponds to the kinetic energy of 2.4 eV, approximately the center position of the observed second hump.

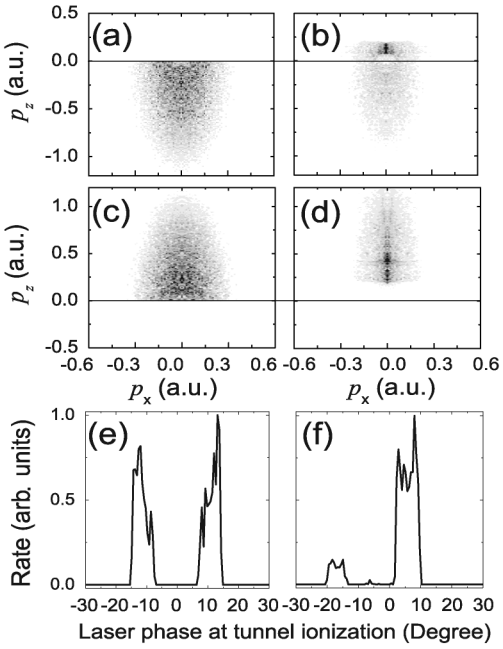

FIG. 2. (a)–(d) Calculated electron momentum distributions (z is the laser polarization direction). $I = 8 \times 10^{13}$ W/cm^2 and $\lambda = 2000$ nm. See the text for the details. (e),(f) Electron yields as a function of the laser phase at the moment of tunnel ionization, without and with the Coulomb potential considered, respectively. Here the statistics are only collected for the electron trajectories that contribute to the energy range of the second hump structure (i.e., $1.0 < E_{\mathrm{kin}} < 3.7$ eV, where E_{kin} is the electron energy) in Fig. 1(b) at $I = 8 \times 10^{13}$ W/cm^2.

From Fig. 2(b), it indicates that, in our semiclassical treatment, the first hump comes from the electrons ionized very close to the crest of the field in the rising edge. The trajectories of these electrons, which are expected to leave the ion directly according to the simple-man picture, are significantly changed by the ion potential and hence the electrons may return to the core and interact with it strongly, leading to the intense concentration in the momentum and energy spectra. For the falling edge shown in Fig. 2(d), the electrons returning to the ion with small

kinetic energies will be influenced by the attractive ion potential strongly. Therefore, not only the electrons' transverse momenta but also the final energies of part of these electrons will be changed, resulting in the first concentration region in Fig. 2(d). When the phase of the ionization time increases in the falling edge, the electron returns to the ion with larger kinetic energy and therefore the core potential can no longer change its final momentum in the field direction significantly. However, the same as in the first concentration region, the momenta of these electrons transverse to the field direction are also significantly changed by the ion potential, resulting in electron's accumulation in the field direction. This phenomenon related to the indirect electron can be referred to as the Coulomb focusing effect, which has been studied in the single ionization process [19] and manifests its important role in the double ionization process [20].

To further understand how the Coulomb potential affects the indirect electron dynamics and produces the second hump in the electron spectra, we collect all trajectories that constitute this hump structure and trace back their tunneling ionization times. Without considering the Coulomb potential, the tunneling times are confined in two regions, one in the rising edge and the other in the falling edge, which are symmetric with respect to the origin [Fig. 2(e)]. This is consistent with the simple-man prediction, in which the final electron energy is solely determined by the laser phase when the electron tunnels out. In contrast to this, the distribution of the tunneling time with Coulomb potential included [Fig. 2(f)] shows that most electrons are emitted in the falling edge, i.e., the contributions are mainly from the indirect electron. Moreover, both phase distributions in Fig. 2(f) shift to the left compared to that in Fig. 2(e).

One more intriguing point is that the right boundary of the right phase distribution in Fig. 2(f) is very close to the phase of 12°, the maximum phase at which the tunneled electron may experience multiple returns, in the context of simple-man theory. This agrees with the above analysis that the second hump is due to the Coulomb focusing effect. More details will be given elsewhere.

In conclusion, we have performed an experimental study on ATI of noble gas atoms at midinfrared wavelengths. An unexpected structure has been revealed in the very low-energy part of the measured photoelectron spectra. Resorting to a semiclassical model, which should be more reliable at long wavelengths, we are able to reproduce this peculiar structure and suggest the origin of this structure as a classical Coulomb effect in long wavelength strong-field physics.

We are grateful to Professor M. S. Zhan for many useful discussions. This work is supported by NNSF of China (No. 10674153 and No. 10574019), the National Basic Research Program of China (No. 2006CB806000), and the CAEP Foundation (No. 2006z0202 and No. 2008B0102007).

Note added.—Very recently, a similar experimental observation has been presented by Blaga *et al.* [21].

*xjliu@wipm.ac.cn
†chen_jing@iapcm.ac.cn
‡ycheng-45277@hotmail.com
§zzxu@mail.shcnc.ac.cn

[1] P. Agostini *et al.*, Phys. Rev. Lett. **42**, 1127 (1979).
[2] For a review, see, e.g., W. Becker *et al.*, Adv. At. Mol. Opt. Phys. **48**, 35 (2002).
[3] G. G. Paulus *et al.*, Phys. Rev. Lett. **72**, 2851 (1994).
[4] P. B. Corkum, N. H. Burnett, and F. Brunel, Phys. Rev. Lett. **62**, 1259 (1989); K. J. Schafer *et al.*, *ibid.* **70**, 1599 (1993); P. B. Corkum, *ibid.* **71**, 1994 (1993); G. G. Paulus *et al.*, J. Phys. B **27**, L703 (1994).
[5] L. V. Keldysh, Sov. Phys. JETP **20**, 1307 (1965).
[6] P. Hansch, M. A. Walker, and L. D. Van Woerkom, Phys. Rev. A **55**, R2535 (1997); M. P. Hertlein, P. H. Bucksbaum, and H. G. Muller, J. Phys. B **30**, L197 (1997); G. G. Paulus *et al.*, Phys. Rev. A **64**, 021401 (2001).
[7] See, for example, H. G. Muller and F. C. Kooiman, Phys. Rev. Lett. **81**, 1207 (1998); R. Kopold, W. Becker, M. Kleber, and G. G. Paulus, J. Phys. B **35**, 217 (2002).
[8] R. Moshammer *et al.*, Phys. Rev. Lett. **91**, 113002 (2003).
[9] J. Chen and C. H. Nam, Phys. Rev. A **66**, 053415 (2002).
[10] K. Dimitriou *et al.*, Phys. Rev. A **70**, 061401(R) (2004).
[11] A. Rudenko *et al.*, J. Phys. B **37**, L407 (2004).
[12] A. S. Alnaser *et al.*, J. Phys. B **39**, L323 (2006).
[13] P. Colosimo *et al.*, Nature Phys. **4**, 386 (2008).
[14] Y. Fu *et al.*, Phys. Rev. A **79**, 013802 (2009).
[15] B. Hu, J. Liu, and S. G. Chen, Phys. Lett. A **236**, 533 (1997); J. Chen, J. Liu, and W. M. Zheng, Phys. Rev. A **66**, 043410 (2002); D. F. Ye, X. Liu, and J. Liu, Phys. Rev. Lett. **101**, 233003 (2008).
[16] M. V. Ammosov, N. B. Delone, and V. P. Krainov, Sov. Phys. JETP **64**, 1191 (1986).
[17] Very recently, an *S*-matrix theory with strong-field approximation [H. R. Reiss, Phys. Rev. Lett. **102**, 143003 (2009)] has been employed to account for experimental data at an even longer wavelength of 10.6 μm [W. Xiong *et al.*, J. Phys. B **21**, L159 (1988)], in which a low-energy peak and another broad one at rather high energy were observed. However, the dependence of the two peaks on the specific atom species therein indicates a different mechanism and is not relevant to our case.
[18] D. G. Arbó *et al.*, Phys. Rev. Lett. **96**, 143003 (2006); Z. Chen *et al.*, Phys. Rev. A **74**, 053405 (2006); M. Abusamha *et al.*, J. Phys. B **41**, 245601 (2008).
[19] A. Rudenko *et al.*, J. Phys. B **38**, L191 (2005).
[20] T. Brabec, M. Y. Ivanov, and P. B. Corkum, Phys. Rev. A **54**, R2551 (1996); V. R. Bhardwaj *et al.*, Phys. Rev. Lett. **86**, 3522 (2001).
[21] C. I. Blaga *et al.*, Nature Phys. **5**, 335 (2009).